LANGMUIR

Interfaces: Adsorption, Reactions, Films, Forces, Measurement Techniques, Charge Transfer, Electrochemistry, Electrocatalysis, Energy Production and Storage

Assembly and characterization of a slingshot DNA nanostructure for the analysis of bivalent and bispecific analytes with biosensors

Paul A Hampel, Ralf Strasser, Frank Fischer, and Ulrich Rant

Langmuir, **Just Accepted Manuscript** • DOI: 10.1021/acs.langmuir.8b02124 • Publication Date (Web): 01 Oct 2018

Assembly and characterization of a slingshot DNA nanostructure for the analysis of bivalent and bispecific analytes with biosensors

Paul A. Hampel[1,2], Ralf Strasser[1], Frank Fischer[1], and Ulrich Rant[1]*

[1] Dynamic Biosensors GmbH, Germany

[2] Technische Universität München, Germany

* Corresponding author: rant@dynamic-biosensors.com

The characterization of novel therapeutic antibodies with multi-valent or multi-specific binding sites requires new measurement modalities for biosensors, to discriminate the engagement of antigens via one, two, or even more binding moieties. The presentation of antigens on a sensor surface in a well-controlled spatial arrangement is a prerequisite for the successful interpretation of binding kinetics measurements of multi-valent analytes, but the adjustment of defined distances between immobilized ligands is difficult to achieve in state-of-the-art biosensor systems.

Here, we introduce a simple DNA nanostructure resembling a slingshot, which can be configured with two identical or two different antigens (bivalent or bispecific), which are spaced at a defined distance. We characterize the slingshot structure with a chip-based biosensor using electrically switchable DNA nanolevers, and demonstrate that bivalent and monovalent antibodies selectively interact with slingshots which have been functionalized with two identical or two different antigens, respectively. The dissociation kinetics are quantified in real-time measurements and we show that the slingshot structure enables a clear differentiation between affinity and avidity effects.

Introduction

Surface biosensors based on surface plasmon resonance (SPR)[1–3], biolayer interferometry (BLI)[4], quartz crystal microbalance (QCM)[5] or electro-switchable nanolevers (switchSENSE)[6] are commonly used for the analysis of binding kinetics between interacting molecules. For the development of molecules as new therapeutics, it is important to characterize biophysical parameters such as on-rates, off-rates, affinity, and avidity, which are characteristic for the binding behavior and mode of action of a drug to its target[7]. In the case of monovalent 1:1 interactions, the association and dissociation kinetics follow simple mono-phasic (mono-exponential) time courses and usually can be analyzed well with state-of-the-art

biosensors[8,9]. However, when bivalent (or bispecific) binders like antibodies are investigated, kinetic signals are more complex and often difficult to interpret. When IgG antibodies are used as analytes and flown across a sensor surface modified with antigens, antibodies may bind a single antigen with one arm, or cross-link two antigens via two arms. Hence, the kinetics reflect contributions from affinity and avidity effects and show a biphasic behavior[10–12]. This is a consequence of the fact that conventional immobilization protocols (e.g. EDC/NHS coupling of amino residues on ligands) create a random distribution of ligands on a sensor surface. Although the ligand density on the sensor may be adjusted to higher or lower levels within the detection limits of the used instruments, the stochastic immobilization inevitably results in variations of the local density of antigens. Quasi-ideal situations where only one type of binding – either monovalent or bivalent – occurs on the sensor, cannot exist on surfaces where the antigen attachment is random and the attachment locations of antigens relative to each other are not controlled.

In this work, we introduce a simple DNA nanostructure termed slingshot, which is used to immobilize two antigens on a biosensor surface at a well-defined spacing of 6 nm. The antigens can be of the same kind, or of different kinds to test bivalent or bispecific analytes, respectively. We characterize the assembly of the DNA structure in solution and on-chip. Immobilized slingshots can be repeatedly loaded with antigens, which can bind antibodies and antibody Fab fragments selectively. Further we demonstrate that, in contrast to conventional surfaces featuring randomly distributed antigens, the dissociation behavior of bivalent analytes from antigens presented on a slingshot shows mono-phasic kinetics. The results suggest that antibodies bind antigens presented by the slingshot with both arms simultaneously, making it straightforward to investigate avidity effects.

Results and Discussion

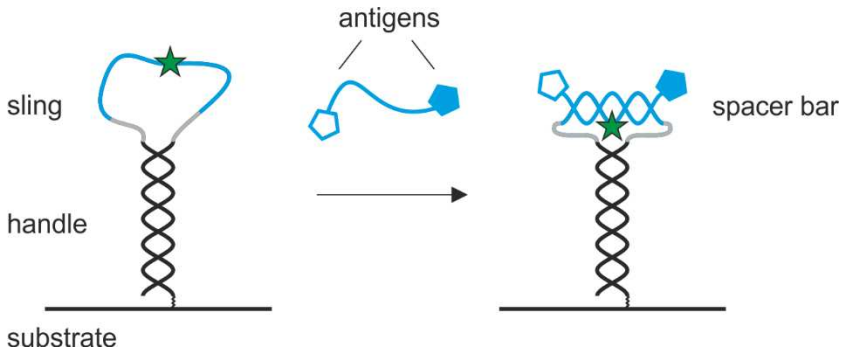

Scheme 1 | Slingshot DNA nanostructure with exchangeable antigens for binding bivalent or bispecific analyte molecules.

Scheme 1 illustrates the slingshot DNA nanostructure: a continuous sequence of 90 nucleotides (nt) forms a rigid double-stranded handle of 30 base-pairs (bp) and 30 nt single stranded sling. The sling is loaded with two antigens by hybridizing a 20 nt complementary sequence (c-spacer, blue) to it, which connects the two antigens. As a result, a rigid spacer bar is formed which keeps the antigens at a defined distance from each other. This spacing can be varied by adjusting the length of c-spacer and sling. The two joint segments connecting the spacer bar to the handle (shown in grey) are single stranded $(dT)_5$ homo-nucleotide stretches in order to avoid base-stacking interactions and allow for flexibility[13]. At its center, a Cy3 dye is conjugated to the sling by internal modification for fluorescence detection.

At first, we characterize the modular composition of the slingshot structure in solution. **Figure 1A** depicts fluorescence resonance energy transfer (FRET) measurements to confirm that the c-spacer sequence correctly hybridizes to the sling. To this end, the c-spacer was labeled at its central position with Cy5, which acts as an acceptor for non-radiative energy transfer from optically excited Cy3 fluorophores. Solutions containing only Cy3-labelled sling or Cy5-labelled c-spacer feature the typical spectra of the respective fluorophores. By contrast, the mixture of both sequences exhibits enhanced (suppressed) emission of Cy5 (Cy3), as it is anticipated if Cy5 is held in close proximity to Cy3 by a c-spacer sequence which is bound to the sling. The FRET efficiency calculated from the measured spectra is 0.7, which corresponds to the maximal efficiency which can be expected under these experimental conditions[14,15].

This suggests a hybridization efficiency close to 100%, meaning that almost all slings are loaded with c-spacers.

To characterize the thermodynamic properties of the DNA nanostructure, we performed melting experiments in solution. The denaturation from a double- to a single-stranded conformation was monitored by absorption measurements at 260 nm, using the hyperchromic effect. For the unloaded slingshot structure (without c-spacer, black line in **Figure 2B**) we find two transitions with melting temperatures $T_{m,1} = 77°C$ and $T_{m,2} = 70°C$. By comparison with thermodynamic calculations using mfold[16], $T_{m,1}$ can be assigned to the melting of the 30 bp handle with an open sling, while the broader transition around $T_{m,2}$ originates from the melting of the handle in combination with a partly folded sling. The stabilization of the structure by a partly folded sling is not surprising, as calculations suggest at least three different possible secondary structures within the sling. Remarkably though, albeit the handle-&-partly-folded-sling structure features a larger number of base-pairs, it is less stable than the handle-&-open-sling structure, which might result from entropic burden imposed by secondary structures within the sling.

When the 20 nt c-spacer sequence is hybridized to the slingshot (loaded sling, red line in Fig. 2B), a third, broad melting transition can be observed at $T_{m,3} \approx 59°C$. A comparison of experimental data and calculations for 20bp, 18bp, and 16bp c-spacer/sling duplexes suggest that this corresponds to the melting of c-spacer from the sling. Furthermore, it can be deduced that 18 ± 2 bases are paired between the sling and c-spacer. Most likely, strain in the sling's $(dT)_5$ joint segments prevents the outermost nucleotides of the c-spacer from base-pairing. Thus, the rigid spacer length is 18×0.34 nm = 6.1 nm here.

Next, we characterized the slingshot nanostructure on a biosensor surface, employing the switchSENSE method, which uses the electrical actuation of DNA nanolevers to detect proteins[17] and nucleic acids[18]. The method allows to determine both association and dissociation rate constants in real-time[19]. To test whether the structure is suited for this measurement modality, slingshots were immobilized on gold surfaces using thiol modified handles. **Figure 1C** shows that the orientation of the slingshots can be modulated efficiently by applying ±0.4V to the supporting microelectrodes (vs. an ITO counter electrode). The orientation switching is monitored by measuring the fluorescence emitted by Cy3 dyes attached to the sling's center. Whenever the negatively charged slingshots are attracted by positive potentials and lie on the surface, the fluorescence is quenched by non-radiative energy transfer to the gold film[20]. Conversely, when the slingshots are repelled by negative potentials and stand upright, the fluorescence emission is high.

The hybridization of c-spacer to surface immobilized slingshots can be followed in real-time when incubating structures with open slings with solute c-spacer sequences, see **Figure 1D** (for experiments on surfaces, c-spacers were not modified with Cy5 in the center). As c-spacer binds into the sling and forms the double stranded spacer bar, the fluorescence modulation amplitude ΔF decreases because the sling is pulled towards the handle, which reduces the vertical extension of the standing structure (stronger quenching by the gold surface). Association rate constants k_{on}^{obs} were analyzed by fitting single exponential functions ($Signal(t) \propto exp\{-k_{on}^{obs} \cdot t\}$) to kinetic data measured for different concentrations of c-spacer, and the association rate $k_{on} = (5.3 \pm 0.4) \times 10^4 M^{-1}s^{-1}$was determined from a linear fit in **Figure 1E** ($k_{on}^{obs} = c \cdot k_{on} + k_{off}$). This value agrees well with other reports on oligonucleotide hybridization on surfaces[21,22], but is lower than what is expected for hybridization in solution ($k_{on} \sim 10^5 - 10^6 M^{-1}s^{-1}$)[22].

The spacer bar can be regenerated reproducibly by reloading the sling with fresh antigen-modified c-spacer. Rinsing the surfaces with NaOH solution (pH 13) for app. 10 seconds suffices to denature the slingshot structure and removes bound c-spacer sequences. After the pH 13 treatment the handle refolds and the sling can be hybridized with new c-spacer, as can be seen in **Figure 1F**, which depicts 16 regeneration cycles showing good signal stability. For these experiments, c-spacers were modified internally with two additional Cy3 dyes (see Methods), which increased the fluorescence intensity for the hybridized structure. The ratio of the fluorescence intensity loaded:unloaded sling of about 2.7 is in good agreement with solution experiments, which indicates that the hybridization efficiency on the surface is close to 100%.

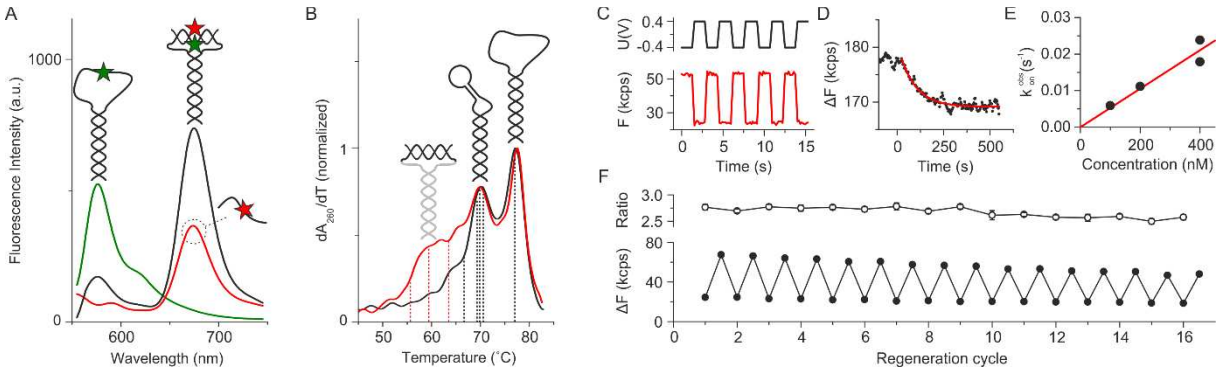

Figure 1 | Formation and regeneration of the slingshot nanostructure. (A) Hybridization of complementary spacer strand (c-spacer) to the sling in solution monitored by FRET. The central nucleotides of sling and c-

spacer were labelled with Cy3 (green, donor) and Cy5 (red, acceptor) dyes, respectively. Green and red lines are spectra of individual slingshot and c-spacer sequences in solution, the black line is a mixture ($c_{slingshot}$=90nM, $c_{c\text{-}spacer}$=100nM, λ_{exc}=530 nm). **(B)** Melting analysis of slingshot sequences with (red) and without (black) added c-spacer by UV hyperchromism in solution (c_{DNA}=1µM). Dashed vertical lines are calculated melting temperatures. **(C)** Electrical orientation switching of slingshot structures on a gold surface. The Cy3 fluorescence F is high for standing, and low for lying orientations, respectively. **(D)** Real-time measurement of the hybridization of c-spacer sequences (200 nM) to slingshot structures immobilized on gold surfaces. ΔF is the fluorescence modulation amplitude of the electrically actuated slingshot structure. The solid red line is a single exponential fit, from which the rate constant k_{on}^{obs} of hybridization is analyzed. **(E)** k_{on}^{obs} as a function of c-spacer concentration in solution. **(F)** Regeneration: repeated removal of c-spacer sequence from immobilized slingshot structures by pH13 denaturation and re-hybridization with fresh c-spacer. The upper panel depicts the ratio between slingshot loaded with c-spacer and unloaded slingshots.

To assess the selective binding of analytes to antigen-modified slingshot layers, we analyzed different binding states, cf. **Figure 2**. Two different small molecules were used as antigens, biotin (bio) and digoxigenin (dig), and three spacer bar variants were investigated: bio-spacer-bio, dig-spacer-dig, and dig-spacer-bio. As analytes with one or two binding sites, we used monovalent anti-bio Fab, monovalent anti-dig Fab, and bivalent anti-bio IgG.

The slingshots' binding states are analyzed by a time-resolved measurement that allows us to gauge the size of bound analyte from the slingshot orientation-switching dynamics[17]. **Figure 2A** shows time-resolved fluorescence upward switching traces of slingshot structures before and after binding analytes of different sizes (Fab≈50kDa, Fab+Fab≈100kDa, Fab+IgG≈200kDa). Due to their greater hydrodynamic friction, larger analytes slow the switching dynamics to a greater extent and the time-resolved fluorescence curves are less steep. For straightforward analysis, time-resolved curves are converted to single numbers, the Dynamic Response (DR), representing a switching 'velocity': the DR parameter equates to the integral under the curves (cf. Fig. 2A)[17]; it decreases when analytes bind to the sling and slow down the switching dynamics of the slingshots.

Figure 2B exemplifies the sequential binding of anti-dig Fabs and anti-bio IgGs to a layer of slingshots loaded with bispecific dig/bio spacer bars. The analyte concentrations were chosen well above the dissociation constant (K_D) to ensure saturation of all surface binding sites ($K_D < 0.1nM \ll c_{Fab,IgG} = 10nM$). As can be expected from their different sizes, the binding of full

antibodies results in a greater signal change than the binding of Fabs. Because the association kinetics were limited by mass-transport in these experiments, the transitions are quasi-linear.

In order to assess the selectivity of the antibody – slingshot interactions, we performed a combinatorial set of experiments where monovalent (anti-dig Fab, anti-bio Fab) and bivalent (anti-bio IgG) analytes were bound to bispecific (dig/bio) or bivalent (bio/bio, dig/dig) spacer bars in different order. The schematics below **Figure 2C-H** illustrate the different binding situations. Distinct binding states can be discriminated by the Dynamic Response values, which scale in magnitude with the total size of bound analyte ($\Delta DR_{Fab} < \Delta DR_{Fab+Fab} < \Delta DR_{Fab+IgG}$). The bivalent IgG is an exception (cf. Fig. 2G): although its molecular weight exceeds that of two Fabs, ΔDR_{IgG} is smaller than $\Delta DR_{Fab+Fab}$. This indicates that the hydrodynamic friction of a flexible construct, where two Fabs are individually bound (Fig. 2E,F) to the slingshot, is greater than that of a rigid structure where one IgG is connected to the spacer bar by both arms in a rigid manner (Fig. 2G). Overall, binding to the slingshot spacer bar is found to be site-specific and does not depend on the succession of binding events.

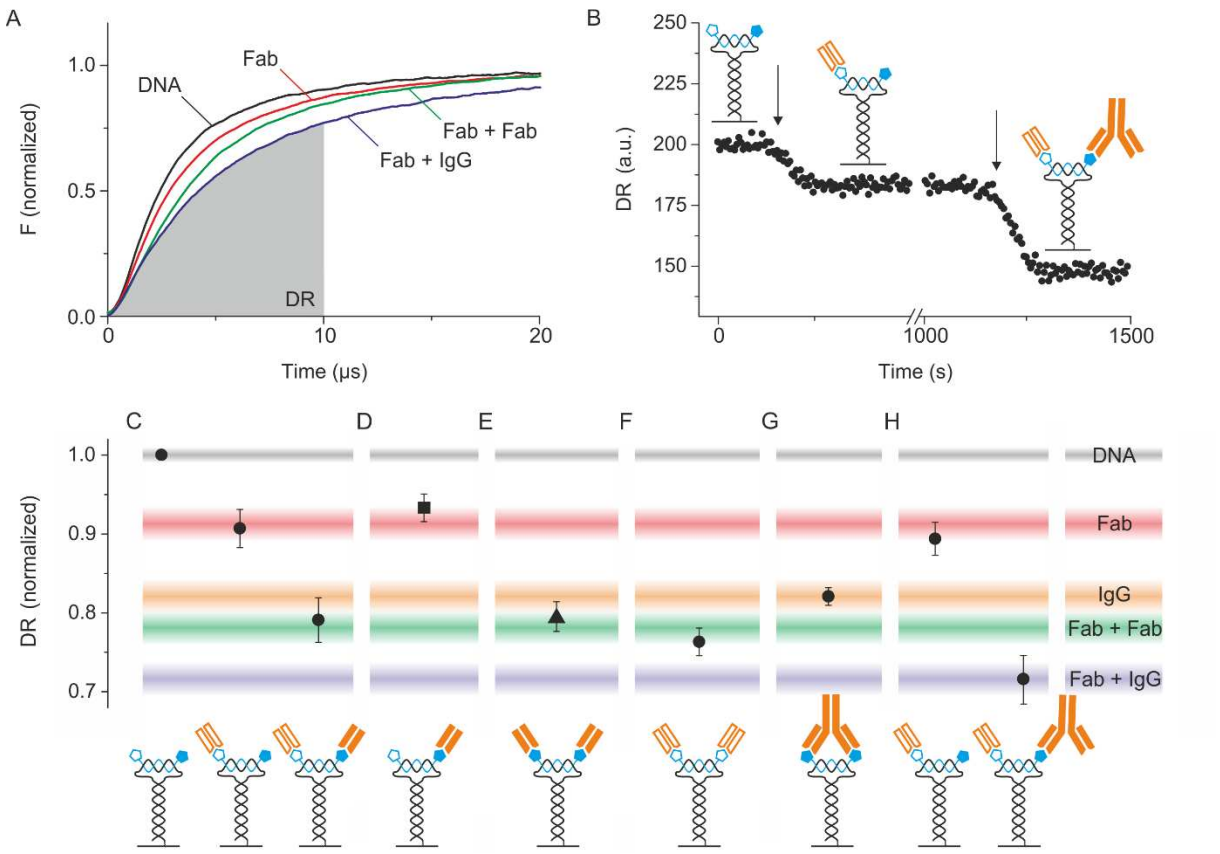

Figure 2 | Binding response of full IgGs and IgG-fragments (Fab) to slingshot structures modified with two identical or two different antigens. (A) Time-resolved fluorescence signal during the upward orientation switching of slingshot levers driven at 10 kHz and ±0.4 V. The Dynamic Response parameter (DR, area under the time-resolved fluorescence trace) is a number representing the switching dynamics; high DR values denotes fast switching. **(B)** Exemplary real-time binding response of Fabs and IgGs binding bispecific (dig/bio) slingshot levers. **(C-H)** Equilibrium binding signals of nanolevers loaded with different combinations of Fab fragments and full IgGs. Open symbols denote dig/antidig, full symbols denote biotin/antibiotin. DR values are normalized by the DR of bare slingshot nanolevers. The spacer bar was labelled with three Cy3 dyes (not shown).

Next we investigated the dissociation behavior of bivalent antibodies, to determine if the slingshot structure is a suitable means to realize well-defined, i.e. mono-phasic, unbinding kinetics. To this end we compared layers of bivalent slingshot probes to the conventional situation where monovalent antigen probes are randomly located on the surface.

For conventional sensor surfaces, where antigens are immobilized in a random fashion, the dissociation behavior of bivalent IgG analytes does not follow a simple mono-exponential time course, but exhibits biphasic dissociation kinetics (**Figure 3A**). This biphasic dissociation behavior of bivalent antibodies has also been observed with SPR biosensors[11]. A double-exponential function of the form $DR(t) \propto A_1 \cdot exp\{-k_{off,1} \cdot t\} + A_2 \cdot exp\{-k_{off,2} \cdot t\}$ is used to fit the data by nonlinear regression. Here, $k_{off,1} = 10.0\ (2.0) \times 10^{-4}$ s^{-1} and $k_{off,2} = 0.63\ (0.03) \times 10^{-4}$ s^{-1} are the dissociation rate constants of two independently dissociating species.

The two off-rates can be assigned to dissociations of IgGs which are bound to one antigen (fast $k_{off,1}$) via one arm or two antigens (slow $k_{off,2}$) via two arms, respectively (see cartoon inset in Fig. 3A). In the latter case the bivalent IgG must interlink two antigen modified probes within its reach. We could confirm the appearance of interlinking in other experiments where the amplitudes of the slow and fast dissociations were studied as a function of the density of antigen probes (data not shown). The contribution from the slowly dissociating species was found to scale with the antigen density, verifying that the slow $k_{off,2}$ stems from IgGs which are doubly bound by interlinking.

In contrast to the more complex biphasic behavior of conventional layers, the dissociation kinetics from layers of bivalent slingshot structures proceeds in a simple, monophasic manner (**Figure 3B**). A single-exponential function describes the slingshot data well, yielding a $k_{off} = 0.33\ (0.02) \times 10^{-4}$ s^{-1} which is comparable to the $k_{off,2}$ obtained for IgGs interlinking two randomly located probes on the conventional layers. A fast $k_{off,1}$ like it has been observed for the conventional layer is not observed for

the slingshot layer, which suggests that all IgGs are bound via both arms to the antigens on the slingshot structure and a singly bound species does not exist on the slingshot layer. The presentation of two antigens on the same probe (slingshot structure) seems to strongly facilitate the engagement via both antibody arms, and thus avidity is the dominant binding mode on the slingshot surface.

As a minor, yet interesting dissimilarity it is noticeable that the bivalent binding avidity is two times more stable on the slingshot than on the interlinked nanolevers of the conventional surface. Presumably, the interlinking of two individual nanolevers, which are subjected to Brownian and electrical actuation, gives rise to tensile stress on the antigen-antibody bond and accelerates the off-rate. On the contrary, the slingshot structure presents the antigens to the antibody in a stable steric configuration with minimal mechanical stress.

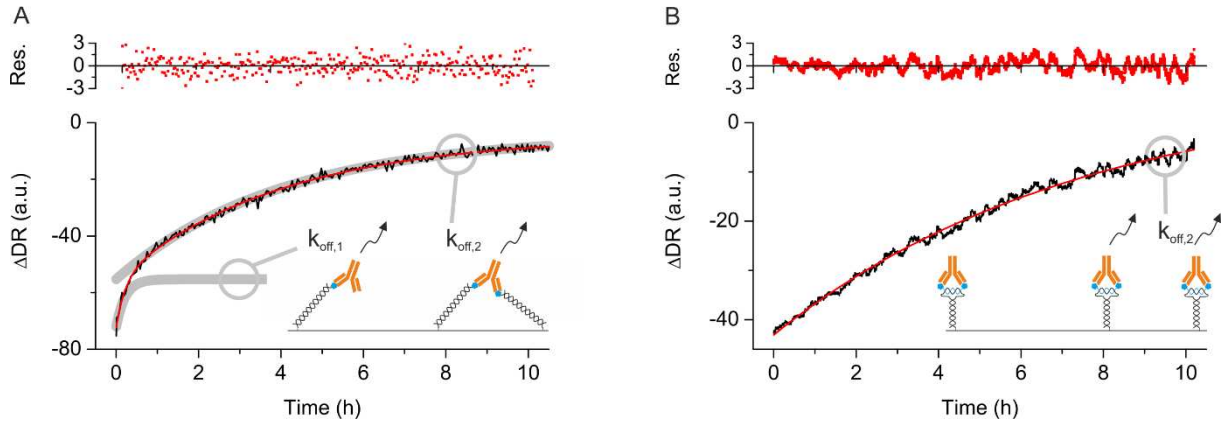

Figure 3 | Dissociation kinetics analysis. (A) Dissociation of bivalent antibiotin IgG from biotinylated probe nanolevers. The red line is a double-exponential fit, thick gray lines are plots of the two individual single-exponential functions, which add up to the double-exponential fit line. **(B)** Dissociation of antibiotin from bivalent slingshot probes. The red line is a single exponential fit. Residuals are shown above the figures.

Table 1: Dissociation rate constants of anti-biotin antibodies from conventional nanolevers and slingshot structures

		Nanolever probe	**Slingshot probe**
Fab[1]	*Fit model*	single exp.	single exp.

	$k_{off,1}$ (10^{-4} s^{-1})	4.5 ± 0.5	3.8 ± 0.4
	Fit model	double exp.	single exp.
IgG[2]	$k_{off,1}$ (10^{-4} s^{-1})	10.0 ± 2.0	n.a.
	$k_{off,2}$ (10^{-4} s^{-1})	0.63 ± 0.03	0.33 ± 0.02

[1] monovalent Fab fragment of polyclonal anti-biotin IgG. [2] bivalent monoclonal anti-biotin IgG.

Table 1 summarizes the rate constants obtained for dissociations of the bivalent IgG and also lists the off-rates for a control experiment using a monovalent Fab fragment (note that the commercially obtained Fab fragment is from a different, poly-clonal anti-biotin IgG, hence the off-rates of the Fab and the IgG cannot be compared quantitatively). Monovalent anti-biotin-Fab fragments dissociate both from the standard layer and the slingshot layer in a monophasic manner with comparable dissociation rates. This is expected, as the monovalent interaction reflects the affinity and does not include contributions from avidity effects.

Summary and Conclusions

In summary, the introduced slingshot architecture is a simple DNA nanostructure that is well suited to be anchored on the surface of a biosensor. The sling can be loaded and regenerated easily with a modular DNA spacer and enables to tether antigens at defined distances from each other. Functionalization of the slingshot structure with two same antigens as well as two different antigens is straightforward. In switching dynamics measurements which are sensitive to the size of the bound analyte we could show that both antigen were active and could bind analytes (IgGs and Fabs) selectively and independent of the succession of binding events. In contrast to conventional immobilization strategies, where antigens are randomly located on the surface, it could be demonstrated that the slingshot structure predominantly bound bivalent IgG analytes via engagement of both arms simultaneously, resulting in an avidity-only binding mode. In the context of antibody sensing with DNA-based structures, the groups of Plaxco and Ricci have demonstrated the use of DNA-based switches for the sensitive detection of antibodies on surfaces using electrochemical readouts and in solution by fluorescence quenching[23,24]. We envision future applications of the structure for the characterization of bispecific antibody formats, which will facilitate the development of novel therapeutic antibodies.

MATERIALS and METHODS

DNA sequences and antibody samples

The DNA for all experiments were obtained from IBA, Germany. The sequence of the thiolated primary 'handle' strand was 5' SH - $(CH_2)_6$ - TAG TCG CCC GCT GAT ATG GCT GAT TCG TCG TTT TTG CAG CTG G T^{Cy3}G TCG AGA CGG GTT TTT CGA CGA ATC AGC CAT ATC AGC GGG CGA CTA -3', the sequence of the 'c-spacer' was 5' – M1 - CCC GT^{Cy3}C TCG AC^{Cy5}A CCA GCT^{Cy3} GC – M2 – 3'. T^{Cy3} denotes the thymine base used for internal Cy3 modification, C^{Cy5} denotes the cyanine base used for internal Cy5 modification (Cy5 was used for the FRET experiments in solution, Cy3 was used for the biosensing experiments on surfaces). M1 and M2 denote the sites for biotin and digoxigenin modifications. Different combinations of modifications were selected according to the experimental setup. The sequence of the reference DNA for DRX measurements was 5' SH – $(CH_2)_6$ - CTG CAT CAC GAG AGC TGG CAA ATG CTA CCT TTG TTG GAG GGT TCA CAC – Cy3 3' and is labeled at its 3' end by a Cy3 dye. The sequences were selected to minimize unintended formation of secondary structures and cross hybridization.

Anti-biotin IgG (monoclonal) and anti-biotin Fab fragment were purchased from Rockland Inc., anti-digoxigenin Fab fragment was purchased from Roche Diagnostics.

Chip and DNA layer preparation

Experiments were performed using customized chips with 'slingshot' surface modification (Dynamic Biosensors, Germany). Gold microelectrodes were modified with binary monolayers consisting of oligonucleotides and 6-Mercapto-1-hexanol (Sigma Aldrich). The Density of the DNA 'handles' was adjusted by applying negative desorption voltages (e.g. -0.8 V vs. ITO) to obtain optimal switching properties for the DNA nanostructures.

Solution Experiments

Thermal denaturation experiments were performed using a Cary 50 UV-vis absorption spectrometer (Varian, USA) equipped with a temperature controlled holder for 1 cm cuvettes. Temperatures were increased from 25 to 85 °C at a rate of 0.5 °C/min under continuous stirring. The concentration of 'handle' and 'c-spacer' DNA was 10µM, each. FRET experiments were performed using a RF-5301PC spectrofluorophotometer (Shimadzu, Japan) equipped with a temperature controlled holder for 1 cm cuvettes. The concentrations were c_{handle} = 90 nM and $c_{c\text{-}spacer}$ = 100 nM. To facilitate a correct

hybridization and folding state of the DNA samples, the samples were diluted in P40 buffer (40 mM NaCl, 10 mM Tris pH 7.4, 0.05 % Tween 20), heated up to 85 °C for 5 minutes and cooled down slowly to 25 °C at 0.5 °C/min before running the denaturation and FRET experiments.

Biosensor experiments

Experiments were performed with a switchSENSE DRX instrument (Dynamic-Biosensors, Germany) at 25°C, running buffer was a phosphate buffer at pH 7.4 with 40 mM NaCl (P40 buffer, Dynamic Biosensors, Germany). The applied switching potential was ±0.4 V vs. ITO at 10 kHz, the flowrate of dissociation experiments was set to 5 µl/min. To regenerate the sensor surface the chip was rinsed with 50 µL pH13 NaOH regeneration solution (Dynamic Biosensors, Germany) followed by a hybridization of 25µL DNA solution (c = 200 nM).

REFERENCES

(1) van Schie, K. A.; Ooijevaar-de Heer, P.; Dijk, L.; Kruithof, S.; Wolbink, G.; Rispens, T. Therapeutic TNF Inhibitors Can Differentially Stabilize Trimeric TNF by Inhibiting Monomer Exchange. *Scientific Reports* **2016**, *6*, 32747.

(2) Abdiche, Y. N.; Yeung, Y. A.; Chaparro-Riggers, J.; Barman, I.; Strop, P.; Chin, S. M.; Pham, A.; Bolton, G.; McDonough, D.; Lindquist, K.; et al. The Neonatal Fc Receptor (FcRn) Binds Independently to Both Sites of the IgG Homodimer with Identical Affinity. *mAbs* **2015**, *7*, 331–343.

(3) Zhao, H.; Gorshkova, I. I.; Fu, G. L.; Schuck, P. A Comparison of Binding Surfaces for SPR Biosensing Using an Antibody–Antigen System and Affinity Distribution Analysis. *Methods* **2013**, *59*, 328–335.

(4) Jiang, J.; Dong, L.; Wang, L.; Wang, L.; Zhang, J.; Chen, F.; Zhang, X.; Huang, M.; Li, S.; Ma, W.; et al. HER2-Targeted Antibody Drug Conjugates for Ovarian Cancer Therapy. *European Journal of Pharmaceutical Sciences* **2016**, *93*, 274–286.

(5) Leo, N.; Shang, Y.; Yu, J.; Zeng, X. Characterization of Self-Assembled Monolayers of Peptide Mimotopes of CD20 Antigen and Their Binding with Rituximab. *Langmuir* **2015**, *31* (51), 13764–13772.

(6) Lux, G.; Langer, A.; Pschenitza, M.; Karsunke, X.; Strasser, R.; Niessner, R.; Knopp, D.; Rant, U. Detection of the Carcinogenic Water Pollutant Benzo[a]Pyrene with an Electro-Switchable Biosurface. *Analytical Chemistry* **2015**, *87*, 4538–4545.

(7) Renaud, J.-P.; Chung, C.; Danielson, U. H.; Egner, U.; Hennig, M.; Hubbard, R. E.; Nar, H. Biophysics in Drug Discovery: Impact, Challenges and Opportunities. *Nature Reviews Drug Discovery* **2016**, *15*, 679–698.

(8) Rich, R. L.; Papalia, G. A.; Flynn, P. J.; Furneisen, J.; Quinn, J.; Klein, J. S.; Katsamba, P. S.; Waddell, M. B.; Scott, M.; Thompson, J.; et al. A Global Benchmark Study Using Affinity-Based Biosensors. *Analytical Biochemistry* **2009**, *386*, 194–216.

(9) Knezevic, J.; Langer, A.; Hampel, P. A.; Kaiser, W.; Strasser, R.; Rant, U. Quantitation of Affinity, Avidity, and Binding Kinetics of Protein Analytes with a Dynamically Switchable Biosurface. *Journal of the American Chemical Society* **2012**, *134*, 15225–15228.

(10) Müller, K. M.; Arndt, K. M.; Plückthun, A. Model and Simulation of Multivalent Binding to Fixed Ligands. *Analytical Biochemistry* **1998**, *261*, 149–158.

(11) Cooper, M. A.; Williams, D. H. Kinetic Analysis of Antibody–Antigen Interactions at a Supported Lipid Monolayer. *Analytical Biochemistry* **1999**, *276*, 36–47.

(12) MacKenzie, C. R.; Hirama, T.; Deng, S.; Bundle, D. R.; Narang, S. A.; Young, N. M. Analysis by Surface Plasmon Resonance of the Influence of Valence on the Ligand Binding Affinity and Kinetics of an Anti-Carbohydrate Antibody. *Journal of Biological Chemistry* **1996**, *271*, 1527–1533.

(13) Ke, C.; Humeniuk, M.; S-Gracz, H.; Marszalek, P. E. Direct Measurements of Base Stacking Interactions in DNA by Single-Molecule Atomic-Force Spectroscopy. *Physical Review Letters* **2007**, *99*.

(14) Tinnefeld, P.; Buschmann, V.; Weston, K. D.; Sauer, M. Direct Observation of Collective Blinking and Energy Transfer in a Bichromophoric System. *The Journal of Physical Chemistry A* **2003**, *107*, 323–327.

(15) Iqbal, A.; Arslan, S.; Okumus, B.; Wilson, T. J.; Giraud, G.; Norman, D. G.; Ha, T.; Lilley, D. M. J. Orientation Dependence in Fluorescent Energy Transfer between Cy3 and Cy5 Terminally Attached to Double-Stranded Nucleic Acids. *Proceedings of the National Academy of Sciences* **2008**, *105*, 11176–11181.

(16) Zuker, M. Mfold Web Server for Nucleic Acid Folding and Hybridization Prediction. *Nucleic Acids Research* **2003**, *31*, 3406–3415.

(17) Langer, A.; Hampel, P. A.; Kaiser, W.; Knezevic, J.; Welte, T.; Villa, V.; Maruyama, M.; Svejda, M.; Jähner, S.; Fischer, F.; et al. Protein Analysis by Time-Resolved Measurements with an Electro-Switchable DNA Chip. *Nature Communications* **2013**, *4*, 2099.

(18) Rant, U.; Arinaga, K.; Scherer, S.; Pringsheim, E.; Fujita, S.; Yokoyama, N.; Tornow, M.; Abstreiter, G. Switchable DNA Interfaces for the Highly Sensitive Detection of Label-Free DNA Targets. *Proceedings of the National Academy of Sciences* **2007**, *104*, 17364–17369.

(19) Langer, A.; Schräml, M.; Strasser, R.; Daub, H.; Myers, T.; Heindl, D.; Rant, U. Polymerase/DNA Interactions and Enzymatic Activity: Multi-Parameter Analysis with Electro-Switchable Biosurfaces. *Scientific Reports* **2015**, *5*, 12066.

(20) Kaiser, W.; Rant, U. Conformations of End-Tethered DNA Molecules on Gold Surfaces: Influences of Applied Electric Potential, Electrolyte Screening, and Temperature. *J. Am. Chem. Soc.* **2010**, *132* (23), 7935–7945.

(21) Tawa, K. Mismatching Base-Pair Dependence of the Kinetics of DNA-DNA Hybridization Studied by Surface Plasmon Fluorescence Spectroscopy. *Nucleic Acids Research* **2004**, *32*, 2372–2377.

(22) Gao, Y. Secondary Structure Effects on DNA Hybridization Kinetics: A Solution versus Surface Comparison. *Nucleic Acids Research* **2006**, *34*, 3370–3377.

(23) Vallée-Bélisle, A.; Ricci, F.; Uzawa, T.; Xia, F.; Plaxco, K. W. Bioelectrochemical Switches for the Quantitative Detection of Antibodies Directly in Whole Blood. *Journal of the American Chemical Society* **2012**, *134*, 15197–15200.

(24) Porchetta, A.; Ippodrino, R.; Marini, B.; Caruso, A.; Caccuri, F.; Ricci, F. Programmable Nucleic Acid Nanoswitches for the Rapid, Single-Step Detection of Antibodies in Bodily Fluids. *Journal of the American Chemical Society* **2018**, *140*, 947–953.

TOC Graphic